Eddy Resolving Lidar Measurements and Numerical Simulations of the Convective Internal Boundary Layer

Shane D. Mayor, Edwin W. Eloranta, and Gregory J. Tripoli
Department of Atmospheric and Oceanic Sciences, University of Wisconsin
1225 W. Dayton St., Madison, Wisconsin, 53706, USA
phone: 608-263-3127, fax: 608-262-5974, e-mail: shane@lidar.ssec.wisc.edu

1. Introduction

Large-eddy simulations (LESs) provide an attractive way of developing parameterizations for global climate and weather forecast models. This is because they provide 4-dimensional (space and time) information with eddy-resolving resolution which can be used to compute fluxes with sampling errors that are much smaller than those made from in situ measurements. LESs, however, are only viable if we have confidence in their solutions. In particular, high-resolution 4-D measurements are needed to test the LESs ability to accurately simulate the organization of convection such as linear and cellular boundary layer circulations. The objective of our research is to demonstrate the usefulness of volume imaging lidar data in LES validation.

The University of Wisconsin's Volume-Imaging Lidar (UW-VIL) was deployed in Sheboygan, Wisconsin, for the Lake-Induced Convection Experiment (Lake-ICE) during the winter of 1997-98. The site was located within 10 m of the western shore of Lake Michigan to measure the 4-D structure of the internal boundary layer (IBL) that forms over the relatively warm lake during westerly and northwesterly cold air outbreaks. The configuration of the VIL used in Lake-ICE allowed us to record backscatter intensity at 15-m intervals out to 18-km ranges.

2. Large-Eddy Simulation

The University-of-Wisconsin Nonhydrostatic Modeling System (UW-NMS) is our LES code. To simulate the IBL, we use a 6.6 million grid-point domain that is 1.8-km wide in the north-south direction by 12-km in the east-west direction. The western 6 km of the domain is located over snow-covered land and the eastern 6 km over 5.9°C water. The domain has 15-m resolution in all directions. A radiosonde sounding, taken 10 km west of the lidar site, provides a horizontally homogeneous initialization. The sounding is neutral to about 400 m and capped by a strong inversion. Air temperature at the surface over land is $-20°$ C. During the simulation, a shear-driven mixed-layer develops over the land and an intense convective IBL develops over the water. The region along the shore where heat-driven thermals have not reached the height of the top of the shear-driven mixed layer is the IBL.

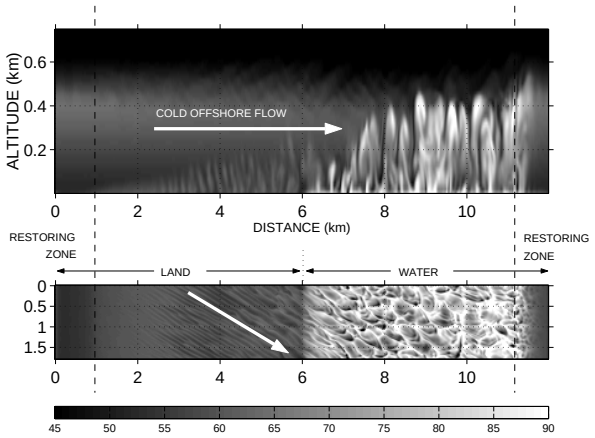

FIG. 1. Relative humidity in the LES at 1-hour after initialization in vertical (top) and horizontal (bottom) slices. The left-half of the domain lies over snow-covered land and the right-half over 5.9°C water.

To satisfy mass-continuity, our domain is periodic in both lateral directions. To restore the flow to the properties of the sounding, 900-m wide vertical "restoring-zones" are installed in the east and west ends of the domain. These zones employ the same numerics as the Rayleigh friction layer in the top of the domain to absorb vertically propagating gravity waves and return model variables to the base state.

To enable comparison with the lidar data, we simulate lidar aerosol backscatter in the LES by using the model's relative-humidity field to quantify optical scattering. Because the lidar uses a log-amplifier, we also take the log of the optical scattering. An approximation of optical scattering from relative humidity was obtained by fitting curves to the observations of Fitzgerald [2]. The absolute magnitude of the scattering is not important for our comparisons because mean values are removed as part of the process to obtain correlation functions and winds.

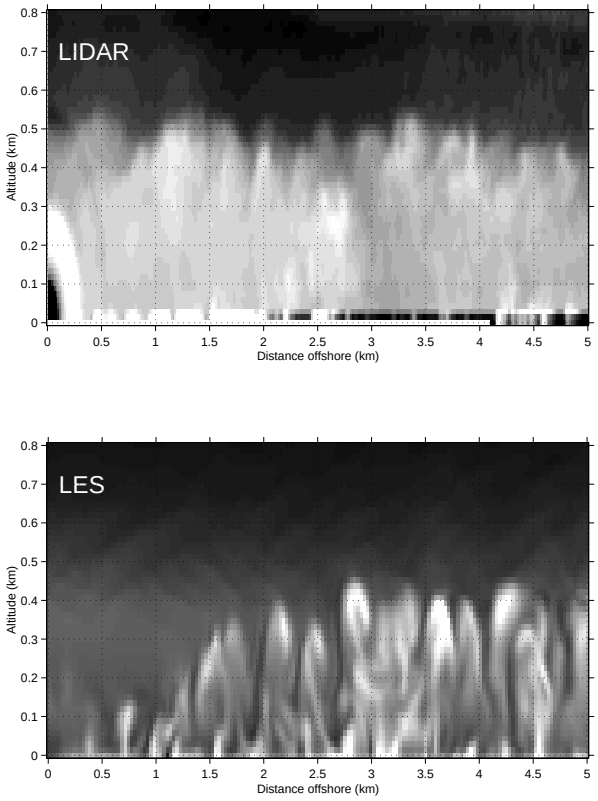

FIG. 2. One RHI-scan of VIL data (top) and a vertical slice through simulated lidar backscatter field in the LES (bottom). Brightness is proportional to aerosol scattering.

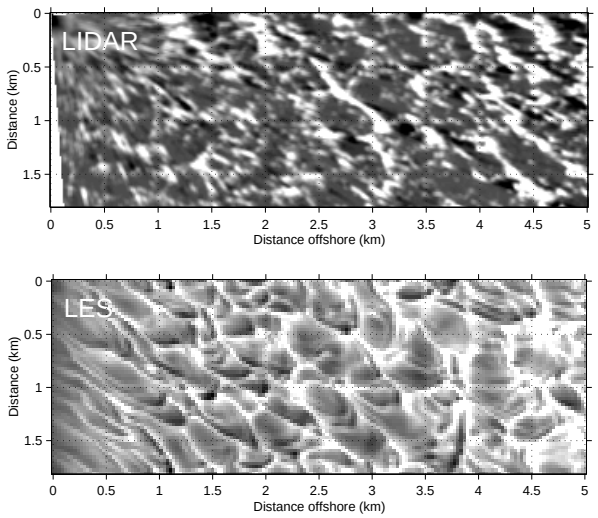

FIG. 3. One PPI-scan of VIL data (top) at 5-m above surface and a horizontal slice through simulated lidar backscatter in the LES (bottom) at 7.5-m above surface.

In fig. 2 the IBL can be identitifed more clearly in the LES than the lidar data. This indicates that the aerosol backscatter is not as strongly dependent on relative humidity as the current parameterization.

In fig. 3 we see similar coherent structures in the comparison of patterns in the aerosol and steam-fog that occurs near the surface. We believe the cellular appearance of the data are caused by the large-eddies impinging on the surface whereby they sweep up heat, moisture and particulates, and confine them to narrow walls of intense rising motion which make up the cells. Many steam-devils were spotted by lidar crew-members during the observations.

3. Lidar measurements of wind

Quantitative measurements of wind can be obtained by cross-correlation of the VIL aerosol backscatter data [1]. In this section, we present spatially resolved wind-fields from the PPI and RHI scans on 13 January 1998. The method described by [1] was applied to square regions, 250-m on a side, to obtain the wind-field shown in fig. 4. This method is similar to the one we describe next for RHI-scans.

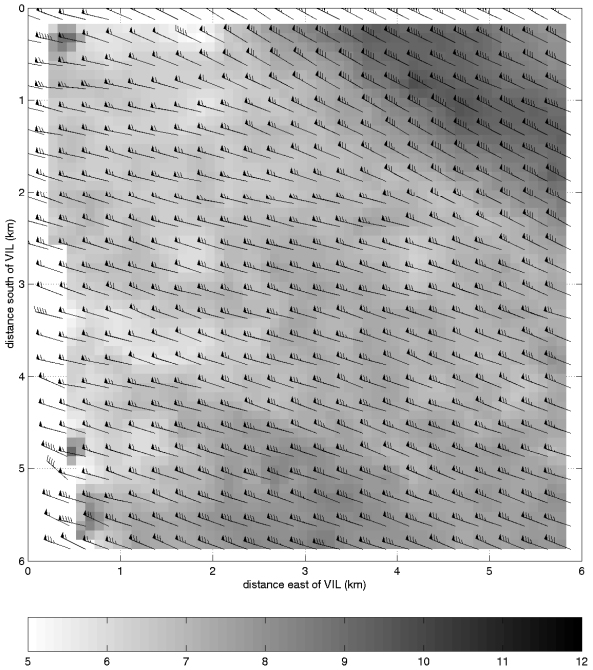

FIG. 4. Wind vectors at 5-m above the lake computed from 40 PPI scans acquired between 10:24 and 10:32 CST on 13 Jan 1998. The background shading is proportional to wind speed in m/s. Meteorological wind barbs are presented with triangles indicating 5 m/s and single barbs indicating 1 m/s.

In an RHI-scan, the time required to scan from zero to 15° elevation and back is about 2 s. To obtain winds from them, the individual lidar returns are high-pass median filtered in range to correct for attenuation. The filtered backscatter-intensity data is then converted from spherical to a cartesian grid with 15-m resolution in both altitude and downwind

distance. At each point in this vertical plane, we compute the spatially lagged cross-correlation function between a value at one time and the value at 20-s later. Each value of the correlation function is obtained by shifting the later frame by one pixel upwind. Correlation functions are accumulated for successive pairs of scans and the position of the peak proportional to velocity. Second degree polynomials are fitted to the peak to improve velocity resolution.

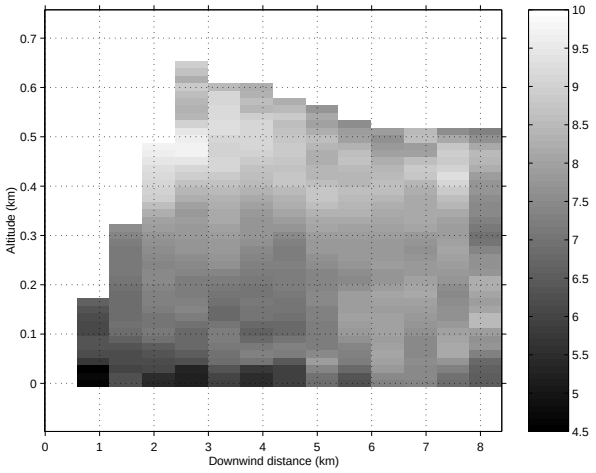

FIG. 5. Downstream-component of horizontal wind-speed in m/s derived from 1290 lidar RHI scans between 10:44 and 11:08 CST on 13 Jan 1998. Correlation functions were summed over 600-m horizontal bands to reduce noise.

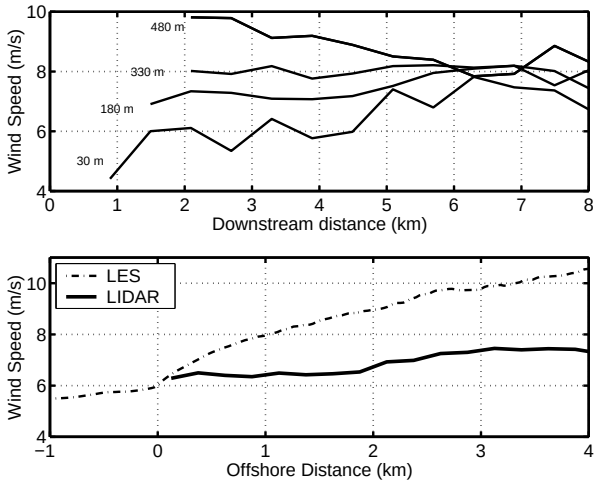

FIG. 6. Lidar RHI-derived wind-speed as a function of downstream distance for four altitudes (top) and lidar PPI-derived wind-speed compared to LES (bottom).

The lidar RHI-derived wind-speeds show the lower levels increasing in speed as a function of downstream distance while the upper levels decrease (top panel of fig. 6). Lidar RHI-scans (and LES (fig. 1) also show the mixed-layer decreasing in depth by about 100-m over 5-km. This is due to subsidence at the inversion level which is caused by offshore acceleration of the flow. The vertical gradient of wind-speed decreases offshore because of strong vertical mixing caused by convection.

The bottom panel of fig. 6 compares the mean lidar PPI-derived wind-speed (5 m above surface) as a function of offshore distance with mean wind-speed from the lowest grid-point in the model (7.5 m). The acceleration of wind in the LES is clearly too high. This may be related to the spatial variation of the wind-field shown in fig. 4 which appears to be caused by the shoreline topography. The wind speed maximum in the upper-right corner appears to be caused by Sheboygan Point which lies directly upwind along the shear-line.

4. Eddy shapes, sizes and lifetimes

Mean eddy size and shape for a fixed distance offshore is obtained by computing the 2-D correlation function of range-corrected backscatter intensity from PPI data according to:

$$R(x, \Delta x, \Delta y) = \frac{\sum S(x,y)S(x+\Delta x, y+\Delta y)}{\sigma_{S_1}\sigma_{S_2} n}$$

where x is the east-west direction and y is the north-south direction. Δx and Δy are lags in 15 m increments here. σ_{S_1} and σ_{S_2} are the standard deviations of the shifted and unshifted arrays. n is the number of points in the arrays.

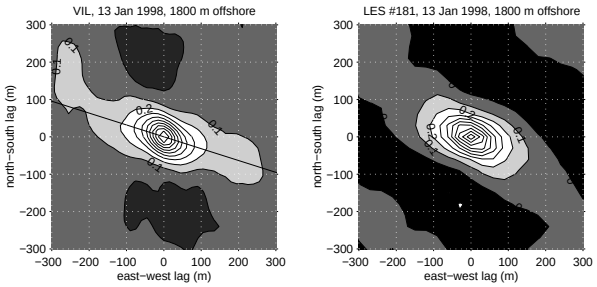

FIG. 7. Two-dimensional correlation function of the aerosol backscatter from the lidar PPI-scans (left) and LES (right) at 1.8 km offshore on 13 Jan 1998. The wind direction was from 287.6° at this range and is indicated by the black line in the left panel.

Fig. 7 shows examples of a 2-D correlation functions of the aerosol backscatter from the lidar PPI-scans and LES at 1.8 km offshore. The ridge of the correlation function runs along the mean wind direction (black line) indicating that the eddies are elongated in the direction of the mean wind. Fig. 8 shows excellent agreement of this along-wind component of the 2-D spatial correlation function for lidar and LES.

By computing the spatial correlation function between scans separated in time, we can see the translating effect of the mean wind and the decorrelating effect of turbulence (see fig. 9). The largest difference between the two sets of curves in fig. 9 is caused by the higher wind speeds in the LES.

Dividing the downwind position of the peaks of the correlation functions by wind-speed allows us to see the decay as a function of time (fig. 10). Some of the offset between the two curves in fig. 10 is probably due to random noise in the lidar data.

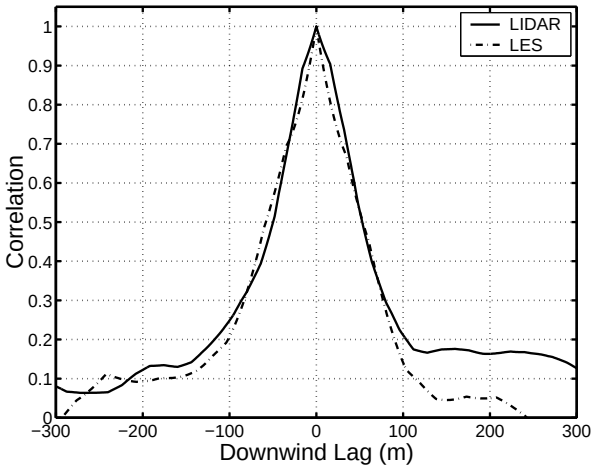

FIG. 8. Comparison of along-wind component of spatial correlation functions for lidar and LES.

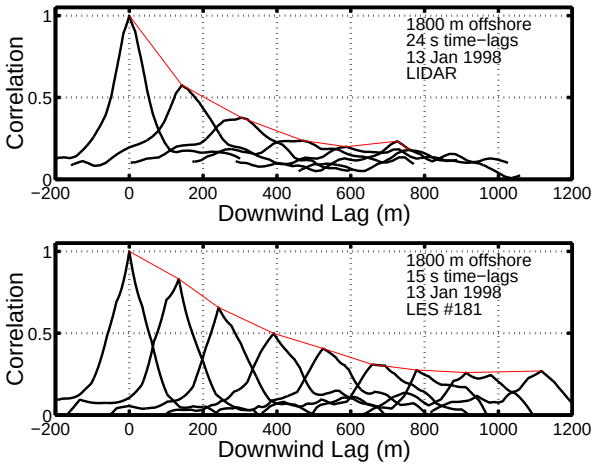

FIG. 9. Along-wind spatial correlation functions obtained from the lidar (top) and from the LES (bottom) for successive time lags.

5. Summary

The simulated eddy structure near the surface is remarkably similar to the lidar data (fig. 3). This similarity is confirmed in spatial correlation functions. Figs. 7 and 8 show that the size and shape of the simulated and observed eddies are nearly identical. Fig 10 shows that the similarity extends to the decay rate of the correlation peak with time.

Acceleration of the wind in the LES is too strong (bottom of fig. 6). This may be related to lack of shoreline topopgraphy in the model. On 10 January 1998 the wind was from the WSW and the observed wind field did not exhibit the topographic induced variation observed on 13 January. Our analysis will be extended to this case.

Our current simulation shows large-eddies of only about half of the observed mixed layer height developing over the 6-km fetch of land in the model. A longer upwind fetch is desirable but is currently limited by computer memory.

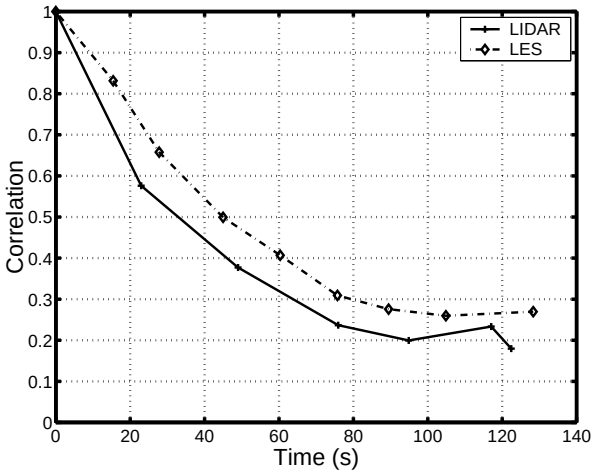

FIG. 10. Comparison of decay of peak correlation as a function of time for lidar and LES at 5-m altitude.

The VIL data from Lake-ICE and LES-output are available as MPEG-movies and gif-files and can be downloaded from our website at http://lidar.ssec.wisc.edu.

References

1. Piironen, A., K. and E. W. Eloranta, 1995: Accuracy analysis of wind profiles calculated from volume imaging lidar data, *J. of Geophys. Res.*, **100**, 25559-25567.

2. Fitzgerald, J. W., W. A. Hoppel, and M. A. Vietti, 1982: The Size and scattering coefficient of urban aerosol particles at Washington DC as a function of relative humidity, *J. Atmos. Sci.*, **39**, 1838-1852.

Acknowledgments

This work was made possible by software written by Joe Garcia and funding from NSF grant number ATM9707165 and ARO grant number ARO DAAH-04-94-G-0195. Simulations performed on a J50 computer donated by IBM.